

Corrosion Behaviour of Polyurethane Coating Containing Fluorocarbon on Carbon Steel in Tropical Marine Atmospheric Environment

Junhang Chen, Jialiang Song, Wei Hu, Taiyang Zhu, Jin Gao, Kui Xiao*

Institute for Advanced Materials and Technology, University of Science and Technology Beijing, Beijing 100083, China

*E-mail: xiaokui@ustb.edu.cn

Received: 23 March 2022/ Accepted: 20 July 2022/ Published: 20 October 2022

To study the corrosion behaviour of carbon steel/fluorocarbon epoxy composite coating materials in a tropical marine atmosphere, outdoor exposure tests of intact and damaged coatings were conducted in Wenchang, Hainan, China. Macroscopic corrosion morphology, glossiness tests, adhesion tests, electrochemical impedance spectrometry (EIS) and scanning Kelvin probes (SKPs) were used to study the performance changes of the intact and damaged coatings after outdoor exposure for 3, 6, 9 and 12 months. The results show that the intact coatings have good protective properties in the tropical marine atmosphere, while the coatings with defects undergo subsurface corrosion. The results show that the carbon steel substrate exposed at the initial stage of corrosion dissolves as the anode and the interface between the metal and the coating is the cathode, which results in the formation of a large amount of OH^- in the alkaline environment, which reduces the adhesion of the epoxy primer to the carbon steel substrate. As the corrosion progresses, a large number of corrosion products are generated at the defects, which makes the potential at the defects move to a new cathode area in a positive direction, and the potential at the adjacent areas moves to a negative direction and becomes a new anode area. The potential difference between the two provides a driving force for the corrosion of the metal under the film. With the accumulation of corrosion products under the film, the adhesion between the epoxy primer and the carbon steel substrate decreases further and finally leads to blistering and peeling failure of the adjacent coating.

Keywords: Marine atmospheric corrosion, Coated carbon steel, Underfilm corrosion

1. INTRODUCTION

The marine atmospheric environment is characterized by high humid heat and high salt fog, and the materials in service in this environment will quickly fail. In a marine atmosphere, there is a high concentration of chloride ions in the air, which can effectively promote the decomposition of the oxide protective film on the surface of the steel, so even stainless steel will be corroded rapidly [1-3]. Anticorrosion coatings are one of the most economical and effective anticorrosion methods in marine

environments because they can resist the corrosion of external corrosive factors. In recent years, the study of corrosion failure of materials in marine atmospheric environments has gradually become the focus of corrosion research. Lin [4] studied the accelerating effect of ammonia on fluorocarbon coatings in a marine atmosphere and showed that ammonia in the atmosphere can diffuse into a weakly alkaline solution and accelerate the degradation of fluorocarbon coatings. Feng [5] studied the degradation of epoxy coatings by salt particles in a marine atmosphere. The results show that salt crystallization in the micropores of the epoxy resin will lead to the collapse of the epoxy resin and cracking on the surface of the epoxy coatings, and ultraviolet radiation will further aggravate this effect. Ramezanzadeh [6] prepared an epoxy composite coating with graphene. The salt spray test showed that the addition of graphene could effectively enhance the shielding property of the coating and significantly improve its corrosion resistance in marine and atmospheric environments.

To evaluate the failure behaviour of the coatings, accelerated ageing tests were carried out by simulating the solar irradiation, temperature, humidity and salt fog in the atmosphere. However, the ageing of the coating in the natural environment is the result of the cooperation of many factors, and the accelerated test in the lab is a single factor, so these accelerated tests cannot reflect the failure behaviour of the coating in the natural environment [7-9]. Therefore, natural exposure tests are the most reliable methods to evaluate the corrosion resistance of the coating in a practical environment. Katayama [10] used a natural exposure test method to evaluate the long-term atmospheric corrosion performance of thermally sprayed Zn-Al coatings in coastal areas. Their results showed that the atmospheric corrosion resistance of the thermally sprayed Zn-Al coating depends on the initial thickness of the coating, and the life of the coating is proportional to the thickness of the coating. Jie [11] studied the degradation behaviour and mechanism of polyurethane coatings in the atmosphere of the South China Sea. The results showed that the adhesion of the coatings was related to their protective properties. Sheng [12] studied the long-term corrosion behaviour of epoxy primer-coated aluminium alloy in a coastal atmospheric environment. The results show that the coating still has a protective effect after 12 years of outdoor exposure. However, most of the research on metal-coating systems has focused on the surface of the coatings, and less attention has been given to the subsurface corrosion behaviour of the damaged coatings.

In this paper, a Q345 carbon steel coating system was tested in Wenchang, Hainan, China. The changes in the surface properties and morphology of the carbon steel coating were studied by using a specular gloss meter and laser confocal microscopy. The change in adhesion of the coating was tested by the pull-out method. Electrochemical impedance spectroscopy (EIS) and an equivalent circuit model were used to evaluate the electrochemical characteristics of the coating, and the potential change in coating defects was analysed by a scanning Kelvin probe (SKP) to study the corrosion failure behaviour of coatings with defects in a marine atmosphere environment.

2. EXPERIMENT

2.1 Materials preparation

A coating on carbon steel was selected as the material for outdoor exposure. All samples were 150 mm × 75 mm × 2 mm in size. The coating was a double-coating system of chromium-free epoxy

primer and fluorocarbon polyurethane topcoat. The thickness of the paint was 90 ± 10 μm , and the thickness of the topcoat is 110 ± 10 μm . Before the test, an Erichsen 426 coating scratch pen (Erichsen, Germany) was used to destroy the coating on some samples.

2.2 Field exposure

The intact coating specimens and damaged coating specimens were exposed at the tropical marine atmospheric corrosion test site in Wenchang City, Hainan Province, China. The specimens were placed at an angle of 45° on a specimen frame facing south. The test cycles of the specimens were 3, 6, 9 and 12 months.

2.3 Characterization

A Nikon digital camera was used to record the macroscopic appearance of the sample before and after the test, and an XGP series portable specular glossometer was used to measure the glossiness before and after the test at a 60° incident angle. Laser confocal microscopy was used to observe the morphology of the defective coatings before and after the experiments.

2.4 Adhesion test

The adhesion test of the complete coating sample was carried out using the positest pull-out adhesion tester (Defelsko Inc., USA), and the spindle size used for the test was 20 mm.

2.5 Electrochemical impedance spectroscopy

The electrochemical impedance (EIS) of the intact coating was tested using a PARSTAT 2273 electrochemical workstation (AMETEK, United States) with a frequency range of 100 kHz - 10 mHz and a disturbance voltage of 20 mV. The electrolytic cell adopted a three-electrode system, with a saturated calomel electrode as the reference electrode and a 20 mm \times 20 mm \times 1 mm platinum sheet as the auxiliary electrode. The working electrode was a coated sample with an area of 1 cm^2 , the electrolyte solution was 3.5 wt.% NaCl solution, and the test temperature was 25 $^\circ\text{C}$.

2.6 SKPFM measurements

The SKP mode of the Princeton M370 microscanning electrochemical workstation was used to analyse the surface potential at the scratches of the coating samples with defects. The distance between the probe and the sample surface was 100 ± 2 μm , the vibration frequency was 80 Hz, and the amplitude was 30 μm .

3. RESULTS

3.1 Macro morphology and gloss

Fig. 1 shows the macroscopic appearance of the intact coating exposed to Wenchang outdoors over different periods. The surface of the coating is still smooth and intact, without discolouration, cracking, blistering, falling off or rusting. Fig. 2 shows the change curve of glossiness and gloss loss rate of the intact coating surface with time. The glossiness of the coating surface fluctuates above 60°, and the glossiness decreases as a whole. However, after 12 months of exposure, the loss of gloss rate of the coating is less than 10%, indicating that the carbon steel coating still has a good protective effect [13].

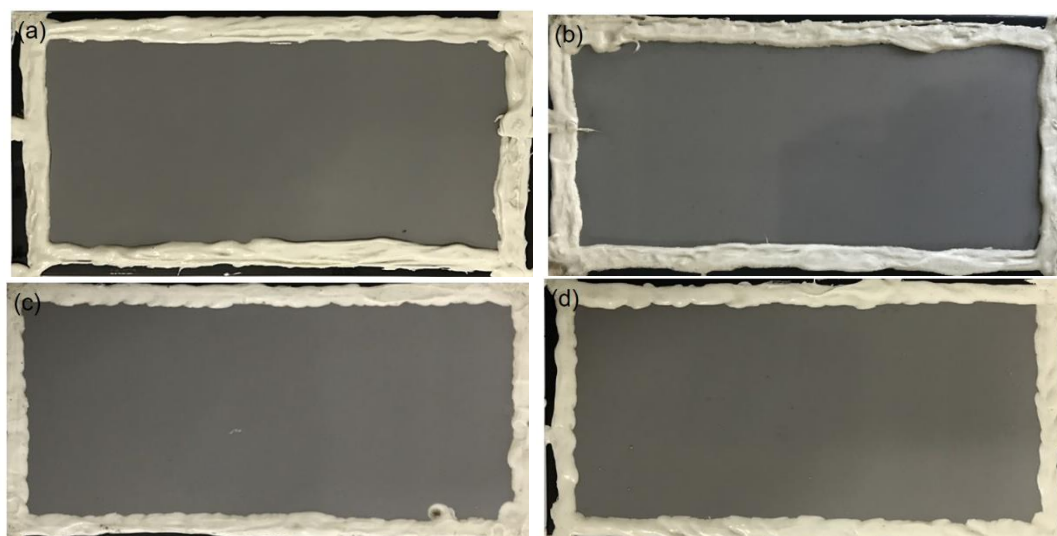


Figure 1. Macro morphology of intact coating samples after exposure for different periods: (a) 3 months, (b) 6 months, (c) 9 months and (d) 12 months.

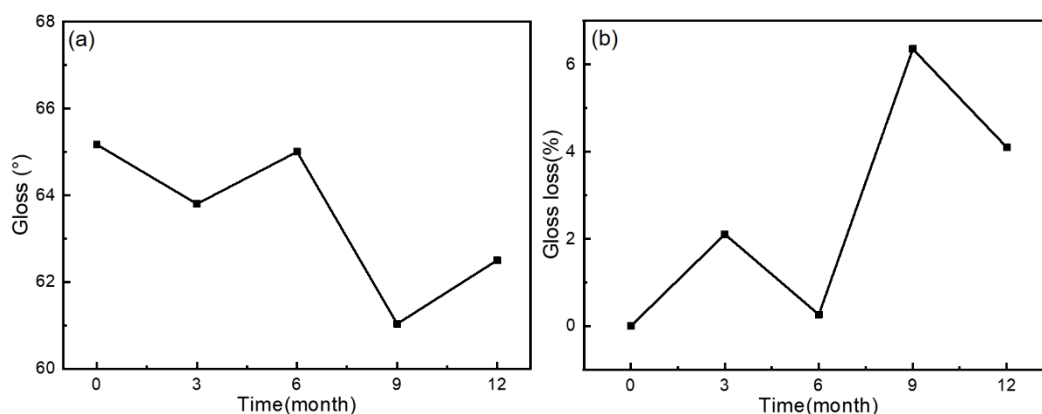


Figure 2. Gloss (a) and gloss loss rate (b) of intact coating sample variation of gloss and light loss rate of intact coating sample.

3.2 Adhesion

The adhesion of the coating is an important parameter to evaluate coating performance. This reflects the interface bonding performance of the coating and determines the service life of the coating equipment [14]. The adhesion of the coating was tested by the pull-off method. Figure 3 shows the appearance after the test. The red epoxy primer indicates that the interface of the epoxy primer/fluorocarbon polyurethane topcoat during the exposure cycle was the weak point of the coating. Fig. 4 shows the adhesion curves of the intact coating exposed for different periods. The adhesion of the carbon steel coating decreases with increasing exposure time, but the adhesion of the coating is more than 6.5 MPa after each period of the exposure test. At this time, the adhesion between the coating and the substrate is still effective and has good corrosion resistance.

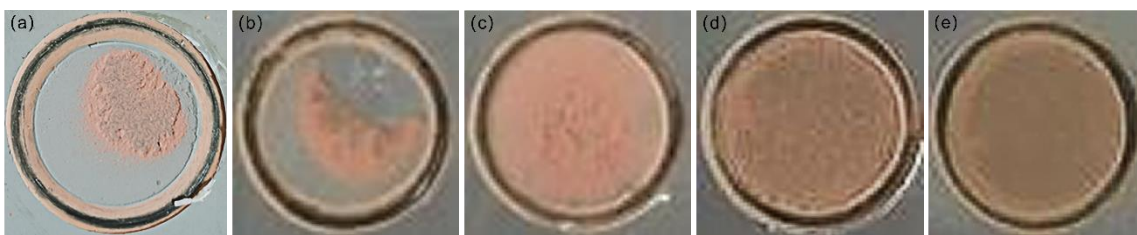


Figure 3 Morphology of coatings with different exposure cycles after the pull-off test: (a) initial sample, (b) 3 months, (c) 6 months, (d) 9 months and (e) 12 months

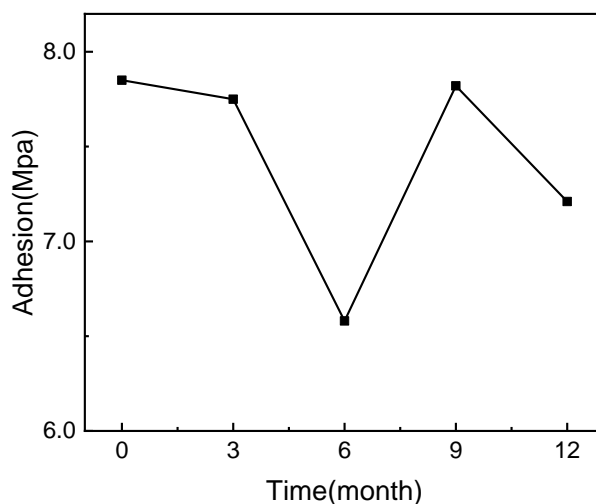


Figure 4. Changes in the adhesion force of intact coatings after different periods of exposure.

3.3 Electrochemical impedance spectroscopy

The EIS characteristics of the intact coating exposed to the outside for different periods of times are shown in Fig. 5. There is no obvious trend of change in the capacitance arc radius of the

coating/carbon steel Nyquist diagram and the low frequency resistance of the Bode diagram ($|Z|$ 0.01 Hz) during the first nine months of the exposure test. After 12 months of exposure, the impedance modulus decreased, but it was still greater than $10^9 \Omega \cdot \text{cm}^2$. Birbilis [15] classified the anticorrosive properties of coatings according to their low frequency impedance modulus. A coating with a low-frequency impedance modulus greater than $10^9 \Omega \cdot \text{cm}^2$ has good protection performance. When the low-frequency impedance modulus of the coating is less than $10^6 \Omega \cdot \text{cm}^2$, the coating is deemed to have failed [16]. In addition, the Bode diagrams of every period show a slope of approximately -1 and no second time constant, which indicates that the coating has better impermeability. The coating is equivalent to an insulating layer with high resistance and low capacitance, and the moisture does not reach the metal interface of the coating/substrate, which indicates a good barrier property.

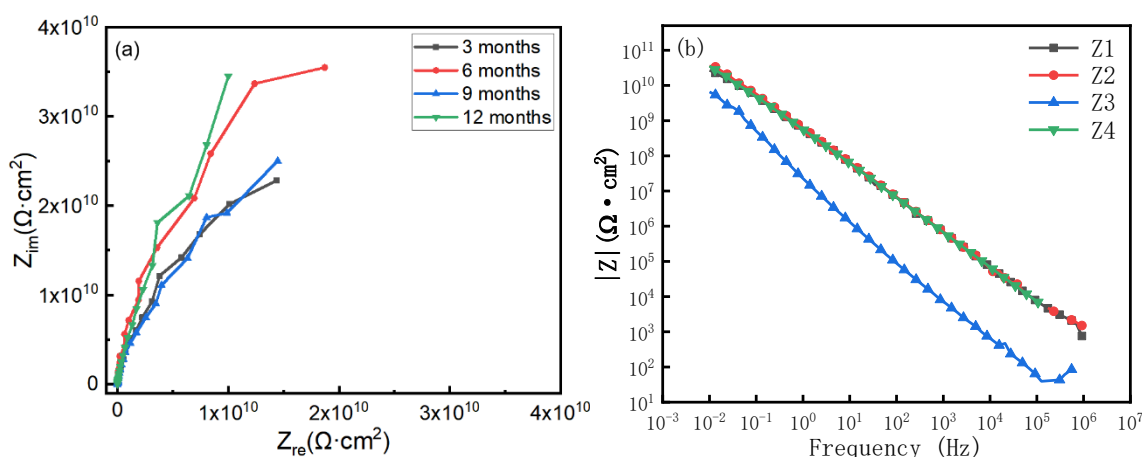


Figure 5. EIS data of the intact coating at different periods in a 3.5 wt.% NaCl solution: (a) Nyquist and (b) Bode modulus.

The EIS spectra of the intact coating were fitted and analysed. The fitting circuit is shown in Fig. 6. R_s is the solution resistance, and R_c is the coating resistance. Considering the nonideal state of the organic coating and the existence of micropores, using Q_c instead of pure capacitance can be more accurate. The resulting fitting parameters are shown in Table 1. The coating resistance and coating capacitance of the carbon steel coating do not change obviously with the outdoor exposure test, which is consistent with the above impedance modulus, indicating that the carbon steel coating still has good protection performance after 12 months of exposure to a tropical marine atmosphere.

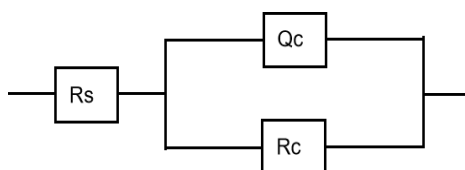


Figure 6. Equivalent circuit model.

Table 1. Electrochemical equivalent circuit element parameters.

Time	Q_c (F/cm ²)	R_c (Ω ·cm ²)
3 months	1.003×10^{-10}	1.531×10^{11}
6 months	8.862×10^{-11}	2.493×10^{11}
9 months	9.763×10^{-11}	1.382×10^{11}
12 months	3.146×10^{-10}	1.044×10^{11}

3.4 Morphological analysis of the scratched surface of the coating with defects

The macroscopic appearance of the defective coating is shown in Fig. 7. After 3 months of outdoor exposure, there is obvious corrosion of the carbon steel substrate at the scratches. After 12 months of outdoor exposure, the edge of the coating scratches is obviously tilted, and a large number of corrosion products are generated on the carbon steel metal substrate, resulting in the peeling off of the coating and metal substrate. After peeling off the scratch, the corrosion propagation behaviour of the carbon steel substrate under the film was observed. The result is shown in Fig. 8. Fig. 9 is a time-dependent curve of the corrosion area of the metal under the coating film calculated by the Photoshop software. The increase rate of the subsurface corrosion area of the scratched coatings is almost constant with time during the first 9 months of exposure, but the increase rate of the subsurface corrosion area of the scratched coatings increases after 12 months of exposure, which may be due to the formation of a large number of corrosion products on the scratched metal substrate, and the tensile stress generated by the corrosion products on the coating accelerates the stripping process of the coatings [17].

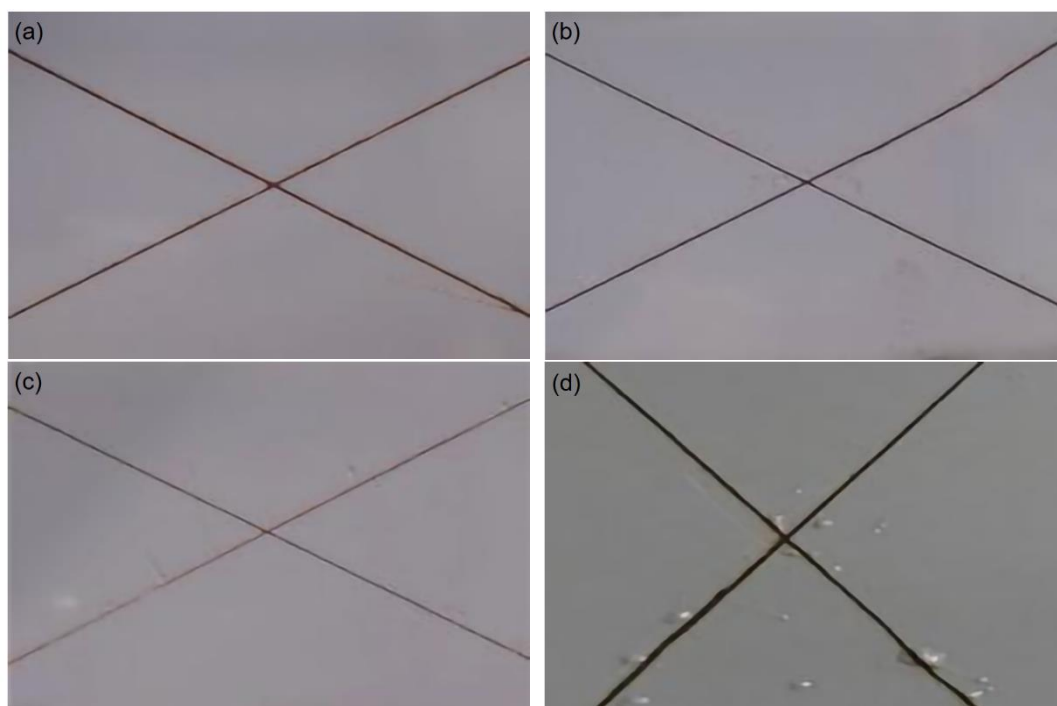


Figure 7. Macroscopic morphology of coated specimens with defects after different exposure periods: (a) 3 months, (b) 6 months, (c) 9 months and (d) 12 months.

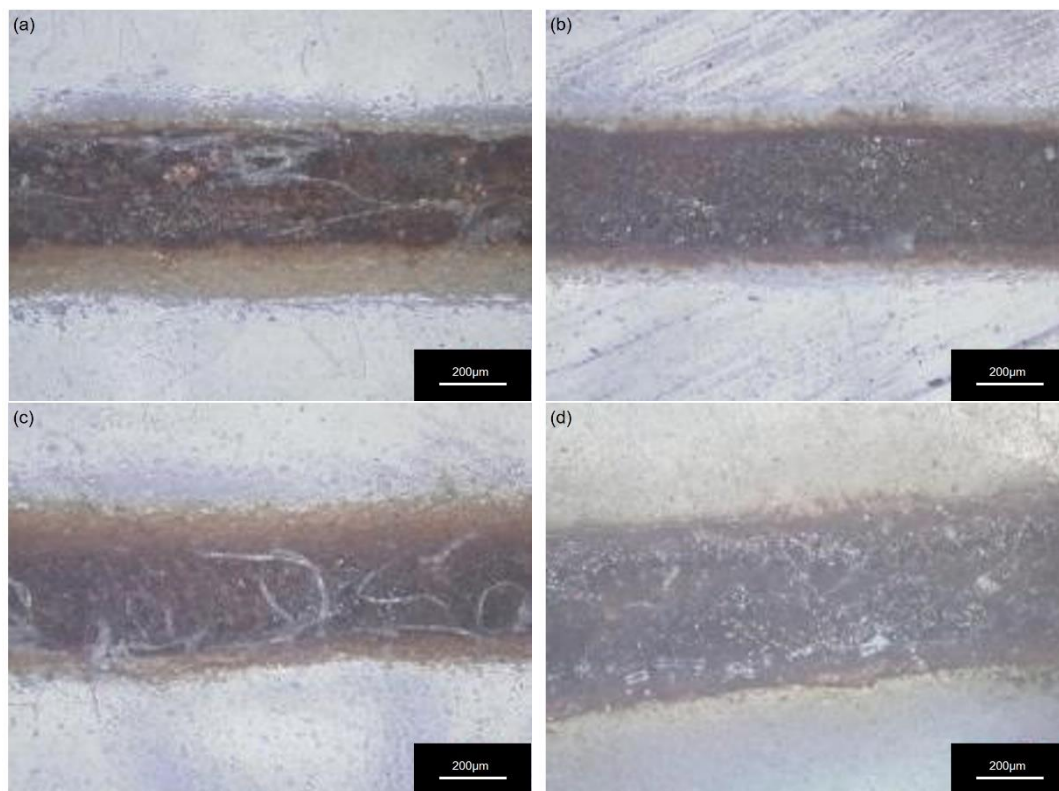


Figure 8. Subsurface corrosion morphology of coated specimens with defects after different exposure periods: (a) 3 months, (b) 6 months, (c) 9 months and (d) 12 months.

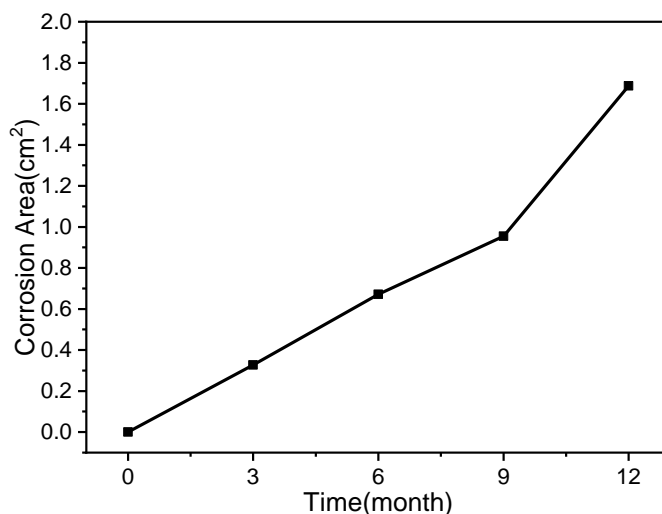


Figure 9. Relationship between the corrosion spread area and exposure time of the coating with defects

The 3D shape of the local area of the scratch is shown in Figs. 10 and 11. After 3 months of outdoor exposure, the surface of the coating at the scratch remains flat; after 6 months, local warping of the coating can be seen; after 9 months, the warping height of the coating at the scratch reached 90 µm, and the growth rate of the warping height of the coating obviously increased; after 12 months of outdoor exposure, the local deformation of the coating at the scratch was quite serious. The deformation in the direction perpendicular to the coating surface at the scratch shows that when the coating is partially

damaged, the substrate at the damaged part will lose the protective effect of the coating, and corrosion will occur under the action of the atmospheric environment. The corrosive factors in the atmospheric environment will invade the metal substrate protected by the coating from the exposed metal substrate, and the corrosion products will break the bond between the coating and the metal substrate and then cause the continuous peeling off of the coating at the damaged part.

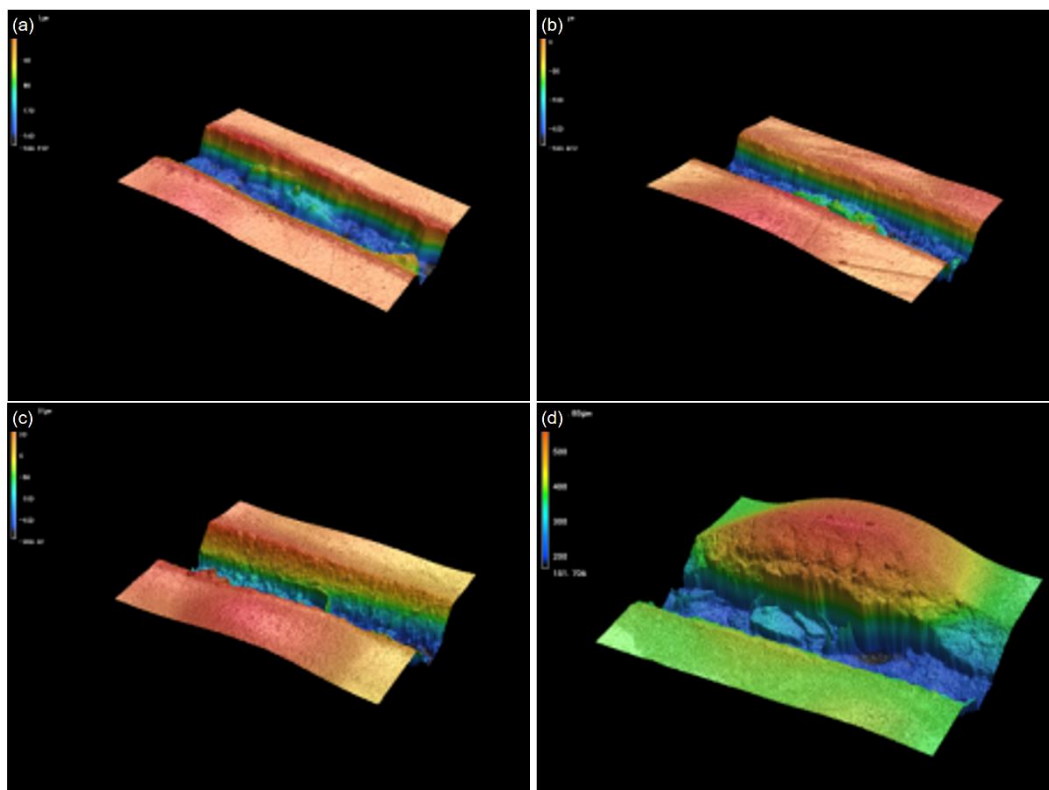


Figure 10. 3D morphology of scratched specimens with defect coatings after different exposure periods: (a) 3 months, (b) 6 months, (c) 9 months and (d) 12 months.

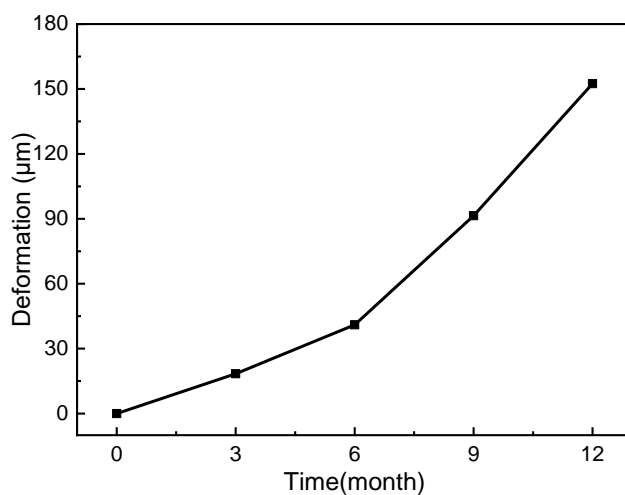


Figure 11. Deformation in the direction perpendicular to the coating surface at the scratch of the coating sample with defects

3.5 Potential Analysis of Damaged Carbon Steel Coating

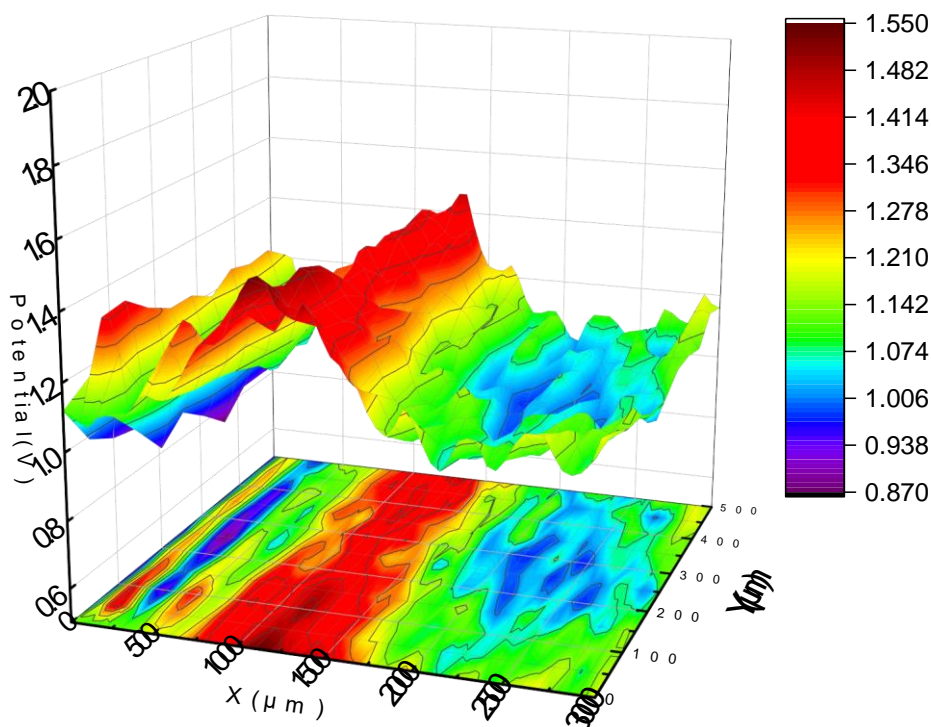


Figure 12. Kelvin potential distribution on the scratched specimen

SKP microelectrochemical measurements were performed on the scratches of the carbon steel-coated specimens after 12 months of outdoor exposure. The Kelvin potential measurements are shown in Fig. 12. The X direction is perpendicular to the scratch direction, and the Y direction is the scratch direction. The middle position of the scratch is the corroded carbon steel matrix, and the two sides are completely coated. The potential of the corrosion area is the most positive at the scratch, and the potential of the intact coating is the most negative. The potential difference between the two is 680 mV. Xiao [18] used a scanning Kelvin probe to study the change in potential with time at the coating defect. It was found that the carbon steel substrate at the scratch of the coating was corroded under an atmospheric environment, and the corrosion product would gradually change the potential at the scratch to a positive value and become the cathode, while the carbon steel substrate below the intact coating around the scratch would become the new anode. The potential difference between the new cathode and the new anode will be the driving force for the further development of subsurface corrosion of the carbon steel.

3.6. Corrosion Mechanism under a Defective Coating Film

The epoxy/fluorocarbon composite coating on the surface of the carbon steel has good adhesion, compactness and insulation and is closely combined with the carbon steel substrate. Due to its good mechanical properties and low surface energy, fluorocarbon topcoats can effectively prevent the infiltration of environmental factors and protect carbon steel substrates. However, when the surface of the coating is damaged, the carbon steel substrate under the coating is exposed to the atmosphere, and

the external environment medium enters the carbon steel substrate surface through the damaged part, causing corrosion of the carbon steel surface. It is generally believed that when the coating is damaged, the exposed carbon steel substrate (anode) and the carbon steel substrate (cathode) under the complete coating film form a corrosive galvanic cell, which accelerates the corrosion of the carbon steel at the coating defect. [19][20] The electrochemical reaction occurring in this scenario is shown in Fig. 13 (a). The cathodic reaction under the coating film produces OH^- that leaves the cathode region in an alkaline environment, destroying the adhesion of the epoxy primer to the carbon steel. At the same time, OH^- will migrate to the defect and form $\text{Fe}(\text{OH})_2$ when Fe dissolves in the carbon steel, but $\text{Fe}(\text{OH})_2$ is not stable. As the corrosion progresses, part of $\text{Fe}(\text{OH})_2$ is oxidized by O_2 , and a corrosion product layer containing FeOOH is formed on the surface of the carbon steel.

The presence of Cl^- in the marine environment can effectively promote the decomposition of thin films on metal surfaces, and Cl^- is more easily adsorbed on metal surfaces than O_2 . Morcillo [21] studied the influence of water-soluble salts at the coating–steel interface on underfilm corrosion, indicating that corrosion-stimulating salts exert an important effect on underfilm steel corrosion and that chloride ions have the greatest influence. Therefore, the unstable $\text{Fe}(\text{OH})_2$ formed in the initial stage of carbon steel at the defect of the coating under the condition of Cl^- will dissolve locally, form a channel in the matrix of the external corrosive medium, promote the continuous extension and development of the corrosion products, and then accelerate the corrosion of the metal matrix.

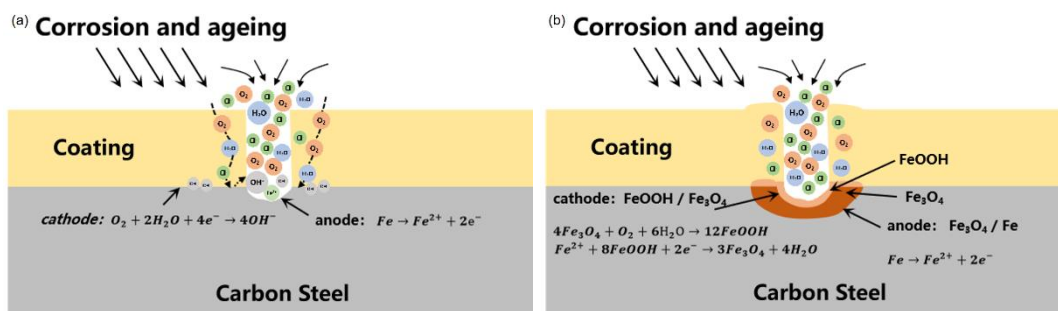


Figure 13. Mechanism of subsurface corrosion of the coating on carbon steel: (a) initial corrosion mechanism of defects and (b) mechanism of underfilm corrosion

With the corrosion of the carbon steel substrate, the early formed FeOOH is easily reduced by Fe^{2+} , and the stable Fe_3O_4 is attached to the holes of the rust layer. Ohtsuka [22] showed that FeOOH and Fe_3O_4 convert to each other as wetting and drying occur, resulting in carbon steel corrosion products that are divided into two layers: loose tan FeOOH and stable Fe_3O_4 in the inner layer. In this process, the state of corrosion products on the surface of carbon steel tends to be stable, which makes the potential move in the positive direction, while the potential moves in the negative direction, which leads to potential reversal of both sides. In this case, the area where the corrosion product is formed in the damaged coating becomes the new cathode, and the carbon steel under the intact coating becomes the new anode. According to the Evans model [23], a cathode reaction occurs at the $\text{FeOOH}/\text{Fe}_3\text{O}_4$ interface, and cathode dissolution of Fe occurs at the submembrane carbon steel/ Fe_3O_4 interface, where the submembrane corrosion mechanism is shown in Fig. 13 (b). The corrosion products formed on the

surface of the carbon steel under the film will accumulate on the interface of the carbon steel and the coating, leading to volume expansion and blistering and providing more channels for the transport of corrosive medium. At the same time, under the action of external water and oxygen, part of the chain in the epoxy coating undergoes hydrolysis, which leads to the overall failure of the coating.

4. CONCLUSION

(1) The exposed carbon steel substrate dissolves as the anode during the early stage of corrosion, and the adjacent interface between carbon steel under the film and the coating undergoes oxygen depolarization as the cathode. The resulting OH⁻ causes the coating to be in an alkaline environment and destroys the adhesion of the coating.

(2) As the corrosion progresses, the corrosion products generated on the surface of the carbon steel substrate at the defect constantly cause the potential at the site to move in a positive direction, while the potential of the metal under the film moves in a negative direction, forming new corrosion anode and cathode areas. The potential difference between the new anode and cathode areas provides a driving force for the subfilm corrosion of the coating.

(3) With the continuous accumulation of corrosion products under the film, the carbon steel/epoxy primer interface expands in volume, forming a channel for the transport of corrosive medium, and the adhesion between the carbon steel and the epoxy primer further decreases under the action of external water and oxygen, resulting in blistering and peeling of the coating macroscopically.

ACKNOWLEDGMENTS

This study was funded by the Science and Technology Project of State Grid Corporation of China (Study on performance evaluation and testing technology of environmentally friendly anti-corrosive coatings for transmission and distribution equipment, 5200-202119092A-0-0-00).

References

1. E. Schindelholz, B. Risteen and R. Kelly, *J. Electrochem. Soc.*, 161 (2014) C460.
2. P. Dhaiveegan, N. Elangovan, T. Nishimura and N. Rajendran, *RSC Adv.*, 6 (2016) 47314.
3. Y. Wang, W. Wang, Y. Liu, L. Zhong and J. Wang, *Corros. Sci.*, 53 (2011) 2963.
4. L. Lu, Z. Ma, Q. Liu and D. Zhang, *Prog. Org. Coat.*, 139 (2020) 105447.
5. Z. Feng, G.-L. Song, Z.M. Wang, Y. Xu, D. Zheng, P. Wu and X. Chen, *Prog. Org. Coat.*, 149 (2020) 105932.
6. B. Ramezanzadeh, S. Niroumandrad, A. Ahmadi, M. Mahdavian and M.M. Moghadam, *Corros. Sci.*, 103 (2016) 283.
7. F. Yang, L. Zhu, D. Han, R. Cao, W. Li, Y. Chen, X. Wang and L. Ning, *Prog. Org. Coat.*, 90 (2016) 455.
8. S. Amrollahi, M. Mohseni and B. Ramezanzadeh, *Prog. Org. Coat.*, 105 (2017) 132.
9. A. Miszczyk and K. Darowicki, *Corros. Sci.*, 43 (2001) 1337.
10. H. Katayama and S. Kuroda, *Corros. Sci.*, 76 (2013) 35.

11. J. Liu, Z. Li, L. Zhang, J. Hou, Z. Lu, P. Zhang, B. Wang and N. Jin, *Prog. Org. Coat.*, 136 (2019) 105310.
12. S. Zhang, Y. He, T. Zhang, G. Wang and X. Du, *Materials.*, 11 (2018) 965.
13. K.A. Wood, *Prog. Org. Coat.*, 43 (2001) 207.
14. D.Y. Perera, *Prog. Org. Coat.*, 28 (1996) 21.
15. R.C. Bacon, J.J. Smith and F.M. Rugg, *Ind. Eng. Chem.*, 40 (1948) 161.
16. Z. Zhang, J. Wu, X. Zhao, Y. Zhang, Y. Wu, T. Su and H. Deng, *Prog. Org. Coat.*, 148 (2020) 105848.
17. N. Birbilis, M. Cavanaugh, A. Sudholz, S.-M. Zhu, M. Easton and M. Gibson, *Corros. Sci.*, 53 (2011) 168.
18. K. Xiao, C.-F. Dong, D. Wei, J.-S. Wu, L.-J. Xu and X.-G. Li, *J. Univ. Sci. Technol. Beijing.*, 33 (2011) 972.
19. D.-H. Xia, J. Wang, Z. Wu, Z. Qin, L. Xu, W. Hu, Y. Behnamian and J.-L. Luo, *Sensors and Actuators B: Chemical*, 280 (2019) 235.
20. Y. Fan, W. Liu, S. Li, T. Chowwanonthapunya, B. Wongpat, Y. Zhao, B. Dong, T. Zhang and X. Li, *Journal of Materials Science & Technology*, 39 (2020) 190.
21. M. Morcillo, F.J. Rodríguez and J.M. Bastidas, *Prog. Org. Coat.*, 31 (1997) 245.
22. T. Ohtsuka and T. Komatsu, *Corros. Sci.*, 47 (2005) 2571.
23. U. Evans and C. Taylor, *Corros. Sci.*, 12 (1972) 227.